



Article

# Cyclodextrin Cationic Polymer-Based Nanoassemblies to Manage Inflammation by Intra-Articular Delivery Strategies

Annalaura Cordaro <sup>1,2</sup>, Roberto Zagami <sup>1</sup>, Milo Malanga <sup>3</sup>, Jagadeesh Kumar Venkatesan <sup>4</sup>, Carmen Alvarez-Lorenzo <sup>5</sup>, Magali Cucchiari <sup>4</sup>, Anna Piperno <sup>2,\*</sup> and Antonino Mazzaglia <sup>1,\*</sup>

<sup>1</sup> CNR-ISMN, Istituto per lo Studio dei Materiali Nanostrutturati, V. le F. Stagno d'Alcontres 31, 98166 Messina, Italy; annalaura.cordaro@ismn.cnr.it (A.C.); roberto.zagami@ismn.cnr.it (R.Z.)

<sup>2</sup> Dipartimento di Scienze Chimiche, Biologiche, Farmaceutiche ed Ambientali, Università di Messina, V. le F. Stagno d'Alcontres 31, 98166 Messina, Italy

<sup>3</sup> CycloLab, Illatos út 7, H-1097 Budapest, Hungary; malanga@cyclolab.hu

<sup>4</sup> Center of Experimental Orthopaedics, Saarland University Medical Center, Kirrbergerstr. Bldg 37, D-66421 Homburg/Saar, Germany; jegadish.venki@gmail.com (J.K.V.); mmcucchiari@hotmail.com (M.C.)

<sup>5</sup> Departamento de Farmacología, Farmacia y Tecnología Farmacéutica, I+DFarma (GI-1645), Facultad de Farmacia and Health Research Institute of Santiago de Compostela (IDIS), Universidade de Santiago de Compostela, 15872 Santiago de Compostela, Spain; carmen.alvarez.lorenzo@usc.es

\* Correspondence: apiperno@unime.it (A.P.); antonino.mazzaglia@cnr.it (A.M.)

Received: 20 July 2020; Accepted: 27 August 2020; Published: 29 August 2020



**Abstract:** Injectable nanobioplatfroms capable of locally fighting the inflammation in osteoarticular diseases, by reducing the number of administrations and prolonging the therapeutic effect is highly challenging.  $\beta$ -Cyclodextrin cationic polymers are promising cartilage-penetrating candidates by intra-articular injection due to the high biocompatibility and ability to entrap multiple therapeutic and diagnostic agents, thus monitoring and mitigating inflammation. In this study, nanoassemblies based on poly- $\beta$ -amino-cyclodextrin (PolyCD) loaded with the non-steroidal anti-inflammatory drug diclofenac (DCF) and linked by supramolecular interactions with a fluorescent probe (adamantanyl-Rhodamine conjugate, Ada-Rhod) were developed to manage inflammation in osteoarticular diseases. PolyCD@Ada-Rhod/DCF supramolecular nanoassemblies were characterized by complementary spectroscopic techniques including UV-Vis, steady-state and time-resolved fluorescence, DLS and  $\zeta$ -potential measurement. Stability and DCF release kinetics were investigated in medium mimicking the physiological conditions to ensure control over time and efficacy. Biological experiments evidenced the efficient cellular internalization of PolyCD@Ada-Rhod/DCF (within two hours) without significant cytotoxicity in primary human bone marrow-derived mesenchymal stromal cells (hMSCs). Finally, polyCD@Ada-Rhod/DCF significantly suppressed IL-1 $\beta$  production in hMSCs, revealing the anti-inflammatory properties of these nanoassemblies. With these premises, this study might open novel routes to exploit original CD-based nanobiomaterials for the treatment of osteoarticular diseases.

**Keywords:** polymeric cyclodextrins; IL-1 $\beta$ ; human marrow-derived mesenchymal stromal cells; rhodamine

## 1. Introduction

Osteoarthritis (OA) is a prevalent, chronic and severe degenerative disease that affects about 50% of the over-sixty population [1]. OA is characterized by alterations in the whole joint (articular cartilage

degradation, bone remodeling and synovial inflammation) that lead to joint instability, failure, intermittent pain and swelling [2]. While various surgical and pharmacological treatments are available in the clinics to control the progression of OA, none of them are able to reproduce the original hyaline articular cartilage in affected patients [3,4]. Even the efficacy and/or safety of already approved drugs and formulations, such as corticosteroids and hyaluronic acid (HA) dispersions, are debated for different reasons: i) the time of residence of free drugs in the joint upon intra-articular administration is inadequate because of adverse pharmacokinetics that behave with rapid lymphatic drainage and physiological turnover of the synovial fluids and ii) the diffusion of drug through cartilage could be slower than its clearance because of the high density of anionic extracellular matrix and small pore size ( $\cong 15$  nm), thus free drugs could not achieve the therapeutic concentrations in the target site. To encompass the rapid clearance of free drug (from hours or few days to weeks) a plethora of engineered biomaterials were proposed [5]. However, sustained intra-articular delivery strategies by means of drug conjugated or entrapped in hydrogels have some limitations such as (i) the chemical modification could inactivate the drug and (ii) the delayed release of a small drug is generally achieved by increasing the crosslinking of the polymer, which could not flow through a syringe and finally not match the mechanical features of the joint [6]. To contrast the short therapeutic time, decreasing the frequency of administration, thus optimizing the cartilage penetration, more injectable nanoformulations based on cationic polyelectrolyte needed to be proposed for intra-articular delivery [7].

Therapeutic polymers are excellent candidates to get suitable nanosize-drug delivery systems with the successful features for OA treatment [8]. Cyclodextrins (CDs) are cyclic oligosaccharides capable of encapsulating guest molecules within their hydrophobic cavity via non covalent interactions. The sequestration of the guest (or part of it) inside the cavity usually improves its physicochemical properties, meanwhile increasing its solubility and protecting it from the aqueous medium (degradative enzymes, oxidants, etc.) [9]. CD polymers show additional properties with respect to their monomeric counterpart. CD units have been copolymerized to different functionalities, conjugated on the side chains or cross-linked in the backbone of polymers [10–12] forming multifunctional nanoconstructs for effective drug and gene delivery *in vitro* and *in vivo* [13,14]. In particular, nanocarriers based on nonionic branched CD polymers such as CD polymers self-assemblies [15], CD associative arrangements [16,17] and CD nanosponges [18,19] have been widely utilized as versatile tools for hosting drugs (i.e., anticancers, antituberculars, antimalarials, phototherapeutics, etc.) within their network and modulating their release *in vitro* [20–24]. Anionic branched CD polymers have been proposed as components of drug eluting systems [25] or fibers for stent coatings [26,27]. In this scenario, branched cationic CD polymers have been designed for several applications. They increase the permeability of drugs to biological membranes [28], easily self-assemble into optimized nanocontainers for efficient intracellular delivery [29], form nanoemulsions for oral delivery [30], or systems for targeting antimicrobial effects in biofilms [31].

Diclofenac (DCF) is one of the most widely prescribed NSAIDs (non-steroidal inflammatory drug) for its analgesic and anti-inflammatory properties. Unfortunately, similarly to other NSAIDs, DCF use is associated with some gastrointestinal (GI) side effects, including ulceration and hemorrhage. In order to mitigate such side effects, DCF has been successfully administered by controlled release systems based on CDs and their supramolecular assemblies [32,33]. The inclusion of DCF inside the CD cavity helps reducing its GI mucosal toxicity and improves the solubility of the drug, enhancing its bioavailability in the site of action and anti-inflammatory effect. The interaction between DCF and CD molecules or CD oligomers by formation of inclusion complexes has already been studied [34–38]. However, the stability of these complexes could be not sufficient for parental/intra-articular administration [39], and strategies using CD nanomaterials might be required to increase the bioavailability and stability of the nanocomplexes [40]. In OA treatment DCF is often used by oral administration to relieve pain and inflammation, however, the topical route is preferred due to fewer systemic side effects with comparable efficacy [41]. Furthermore, it is challenging to track the effectiveness of action of therapeutic nanoparticles in osteoarticular disorders [42].

Among the ongoing research on supramolecular self-assemblies based on CD for controlled drug/gene delivery in osteoarticular regeneration [43,44], here we develop a nanoconstruct based on branched cationic  $\beta$ -CD (Poly- $\beta$ -amino-cyclodextrin, PolyCD) [45] entrapping DCF and anchoring a probe fluorescent (adamantanyl-Rhodamine conjugate, Ada-Rhod) [46] by a supramolecular interaction. Taking advantage of the high affinity of adamantane unit for CD cavities and of the lipophilic feature of Ada-Rhod [47], the proposed PolyCD@Ada-Rhod/DCF nanoassembly has the potentiality to become theranostic. In this study the presence of Ada-Rhod as a doping agent ([CD]:[Ada-Rhod]  $\cong$  33:1 molar ratio) was exploited to study the cellular uptake of the nanoassembly. The biocompatibility of the system was assayed on human bone marrow-derived mesenchymal stromal cells (hMSCs) and the decrease of intrinsic levels of IL-1 $\beta$  production in hMSCs was detected to evaluate the protective activities against proinflammatory responses.

## 2. Materials and Methods

### 2.1. Materials

Poly- $\beta$ -amino-cyclodextrin (PolyCD, Average MW = 25 kDa, CD content 70%) was synthesized at CycloLab (Budapest, Hungary) by cross-linking ad-hoc derivatized  $\beta$ -CD monomer with epichlorohydrin as already reported [45]. A colorimetric Kaiser test [48,49] was performed to spectroscopically establish the quantity of amino groups present in PolyCD, which was estimated to be 0.21 mmol/g (see SI (Supplementary Information)). Adamantanyl-Rhodamine conjugate (Ada-Rhod, MW = 735.5 g/mol) was synthesized as previously reported [46]. Diclofenac sodium salt (DCF, MW = 318.13 g/mol) and all the solvents (analytical grade) were purchased from Sigma-Aldrich (Milano, Italy). All the dispersions used for nanoassemblies preparation and spectroscopic characterizations were prepared in ultrapure water (Fresenius Kabi Italia) or in 10 mM phosphate buffer containing NaCl (137 mM) and KCl (2.7 mM) at pH 7.4 (PBS) at room temperature (r.t.  $\cong$  25 °C). pH measurements were obtained using an 827 pH Lab pHmeter—Metrohm.

### 2.2. Nanoassemblies Preparation

#### 2.2.1. Preparation of PolyCD@Ada-Rhod

The complex was prepared at [CD]:[Ada-Rhod]  $\cong$  33:1 molar ratio (0.017  $\mu$ mol of Ada-Rhod/mg of PolyCD) with [CD] equal to a molar concentration of repetitive units in PolyCD (see SI). Briefly, PolyCD was dissolved in ultrapure water (44 mg/4.4 mL) and sonicated in an ultrasonic bath (10 min). A thin Ada-Rhod organic film (0.6 mg) was prepared by slow evaporation of a dichloromethane (DCM) solution and this latter was hydrated with the previously prepared polymer solution (heated at 50 °C), followed by sonication in ultrasonic bath (1 h 30 min). The pink aqueous phase was collected and analyzed, whereas the residual Ada-Rhod film was separated by slight centrifugation and used to determine Ada-Rhod actual loading into the complex (by difference of the weighted amounts of Ada-Rhod initially present in organic film and the residual film after hydration).

#### 2.2.2. Preparation of PolyCD@Ada-Rhod/DCF

An organic film of DCF (17 mg at [CD]:[DCF] 1:1 molar ratio) previously prepared by slow evaporation of an acetone solution was hydrated with an aqueous solution of PolyCD or PolyCD@Ada-Rhod (92.3 mg/10 mL) and sonicated for 20 min.

All the samples were freeze-dried and then reconstituted in aqueous medium. After freeze-drying, recovery yield was calculated considering the final recovered amount of product (mg) vs. the initial weighed amount of each component.

### 2.3. Loading and Entrapment Efficiency

Both Ada-Rhod or DCF actual loading (AL%), theoretical loading (TL%) and entrapment efficiency percentages (EE%) were evaluated by UV/Vis spectroscopy using the following Equations:

$$AL (\%) = \frac{\text{amount of Ada - Rhod or DCF into the nanoassembly}}{\text{weight of nanoassembly}} \times 100 \quad (1)$$

$$TL (\%) = \frac{\text{amount of Ada - Rhod or DCF initially added to formulation}}{\text{weight of nanoassembly}} \times 100 \quad (2)$$

$$EE (\%) = \frac{\text{amount of Ada - Rhod or DCF in nanoassembly}}{\text{amount of Ada - Rhod or DCF initially added to formulation}} \times 100 \quad (3)$$

The amount of Ada-Rhod loaded into the system was calculated by redissolving the residual film from the complexation reaction in DCM and measuring its absorption intensity. A Lambert and Beer calibration curve for Ada-Rhod in DCM was performed in the concentration range 25–200  $\mu\text{M}$  ( $\epsilon = 877.8 \pm 10 \text{ M}^{-1} \text{ cm}^{-1}$ ; see Figure S1).

DCF actual loading inside PolyCD@Ada-Rhod/DCF system and EE% were evaluated by UV/Vis by means of difference by DCF initially added and residue in organic film after hydration. Calibration curves for free DCF were performed both in ultrapure water and PBS: the calculated molar extinction coefficients were respectively  $8130 \pm 225 \text{ M}^{-1} \text{ cm}^{-1}$  (DCF free in water) and  $9700 \pm 767 \text{ M}^{-1} \text{ cm}^{-1}$  (DCF free in PBS; see Figure S2).

### 2.4. UV/Vis and Steady State and Time Resolved Fluorescence Spectroscopy

UV/Vis spectra were obtained on a Agilent model 8453 diode array spectrophotometer using 1 cm path length quartz cells at  $T = 25 \text{ }^\circ\text{C}$  by using a thermostatic bath. Steady-state fluorescence measurements were performed on a Jasco model FP-750 spectrofluorimeter by using a 0.5 or 1 cm path length quartz cells. Time resolved fluorescence emission measurements were performed on a Jobin Yvon-Spex Fluoromax 4 spectrofluorimeter using time-correlated single-photon counting technique and a NanoLED ( $\lambda = 390 \text{ nm}$ ) as the excitation source, as already reported [50,51].

### 2.5. Job Plot and Characterization of the PolyCD/DCF Complex in Solution

Job's plot experiments were performed by two equimolar stock solutions of PolyCD and DCF ( $[\text{CD}] = [\text{DCF}] = 1 \text{ mM}$ ) both by mixing them in ultrapure water and maintaining the total volume and concentration constant ( $[\text{CD}] + [\text{DCF}] = 100 \text{ } \mu\text{M}$ ) where  $[\text{CD}]$  is the molar concentration of repetitive unit in PolyCD. Accordingly, the molar fraction ( $\chi$ ) was changed from 0.1 to 1 and measuring the corresponding absorbance by UV/Vis at  $T = 25 \text{ }^\circ\text{C}$ . Plots show the  $\chi$  vs.  $\Delta A/A_0 \times [\text{DCF}]$ , where  $\Delta A$  is the difference between absorbance values at maxima in the presence ( $A$ ) and in the absence ( $A_0$ ) of PolyCD respectively vs.  $\chi_{\text{DCF}}$  (where  $\chi_{\text{DCF}}$  is the molar fraction of DCF at the investigated molar concentration  $[\text{DCF}]$ ) [52,53].

The complexation of DCF in PolyCD was studied by UV/Vis titration. Different aqueous solutions of free DCF and DCF with different amounts of PolyCD ( $[\text{DCF}] = 100 \text{ } \mu\text{M}$  and  $[\text{CD}]$  varying in the range 0–150  $\mu\text{M}$ ) were prepared in sealed vials by adding aliquots of PolyCD to aqueous solutions of DCF, homogenized by slight sonication (10 min) and thermally equilibrated at  $T = 25 \text{ }^\circ\text{C}$ . The dispersions were analyzed by UV/Vis as described and the plot of  $1/[A - A_0]$  as a function of  $1/[\text{CD}]$  was reported, where  $A$  and  $A_0$  are the absorbance of DCF in the presence and in the absence of PolyCD measured at  $\lambda_{\text{max}}$  of complex absorbance.

### 2.6. Size and $\zeta$ -Potential Measurements

Hydrodynamic diameter ( $D_H$ ) or size, width of distribution (polydispersity index, PDI) and  $\zeta$ -potential of the PolyCD-based nanoassemblies were determined by photon correlation spectroscopy

(PCS) by a Zetasizer Nano ZS (Malvern Instrument, Malvern, U.K.) at 25 °C in ultrapure water. The measurements were carried out at 173° angle vs. the incident beam at 25 ± 1 °C for each aqueous dispersion. The deconvolution of the correlation curve to an intensity size distribution was obtained by using a non-negative least-squares algorithm. The  $\zeta$ -potential values were measured using a Zetasizer Nano ZS Malvern Instrument equipped with a He–Ne laser at a power  $P = 4.0$  mW and  $\lambda = 633$  nm. The results are reported as the mean of three separate measurements on three different batches ± the standard deviation (SD).

### 2.7. Stability Studies

Stability studies were carried out by dissolving PolyCD@Ada-Rhod/DCF (0.5 mg/mL) in different biological media: (i) ultrapure water, (ii) 0.9 wt % NaCl aqueous solution, (iii) PBS at pH 7.4. All the solutions were kept under stirring ( $T = 25$  °C) along 14 days and analyzed by UV/Vis and DLS at r.t. in triplicate.  $\zeta$ -Potential was measured along 2 weeks on the dispersions prepared in ultrapure water and stored at 25 °C.

### 2.8. Release Studies

Release profile of DCF from PolyCD@Ada-Rhod/DCF nanoassembly was evaluated in PBS at pH 7.4 by a dialysis method. PolyCD@Ada-Rhod/DCF (10 mg) in PBS (1 mL) were put into a dialysis tube (Spectra/Por® dialysis bags, MWCO 3.5 kDa) and immersed into 10 mL of PBS (sink condition) under continuous stirring (250 rpm) at 37 ± 0.5 °C. At fixed times, 1 mL of release medium was withdrawn and replaced with an equal volume of fresh aqueous solution of PBS. The amount of DCF released was evaluated by UV/Vis spectroscopy (at  $\lambda = 276$  nm) and was expressed as percentage ratio between the weight of released DCF and the total amount of entrapped drug. The kinetic analysis was carried by three models proposed in the literature such as Higuchi, Baker–Lonsdale and the first order process (see *infra* and SI) [53,54].

### 2.9. Biological Studies

#### 2.9.1. Materials

All reagents were from Sigma (Munich, Germany) unless otherwise indicated. Recombinant FGF-2 (rFGF-2) was purchased at R&D Systems (Wiesbaden-Nordenstadt, Germany). The Cell Proliferation Reagent WST-1 and the Cytotoxicity Detection KitPLUS (LDH) were obtained at Roche Applied Science (Mannheim, Germany). The Human IL-1 $\beta$  and TNF- $\alpha$  enzyme-linked immunosorbent assays (ELISAs; Human IL-1 $\beta$  Quantikine ELISA, TNF- $\alpha$  Quantikine ELISA) were from R&D Systems.

#### 2.9.2. Cell Culture

Bone marrow aspirates (15 mL) were obtained from distal femurs of patients undergoing total knee arthroplasty ( $n = 8$ , age 68–74 years). The study was approved by the Ethics Committee of the Saarland Physicians Council. All procedures were in accordance with the Helsinki Declaration and all patients provided informed consent before inclusion in the study. Bone marrow-derived human mesenchymal stromal cells (hMSCs) were isolated according to standard protocols [55,56] by washing and centrifuging the aspirates in Dulbecco's modified Eagle's medium (DMEM). The cell pellet was resuspended in red blood cell lysing buffer (Sigma) and DMEM (1:1). The mixture was washed, pelleted and resuspended in DMEM with 10% fetal bovine serum, 100 U/mL penicillin and 100  $\mu$ L/mL streptomycin (growth medium). The cells were plated in T75 flasks and kept at 37 °C under 5% CO<sub>2</sub> overnight. The medium was then removed and replaced by growth medium with recombinant FGF-2 (1 ng/mL), with medium exchanged every 2–3 days. Proliferating cells were replated when reaching an 85% density and hMSCs were further used at no more than passage 1–2. Cell studies were carried out by adding PolyCD-based nanoassemblies (2 mg/mL, [Ada-Rhod] = 32  $\mu$ M, [DCF] = 944  $\mu$ M).

### 2.9.3. Detection of Live Fluorescence

hMSCs were seeded in 24-well plates ( $2 \times 10^4$  cells/well) with growth medium for 12 h at 37 °C under 5% CO<sub>2</sub>. PolyCD-based nanoassemblies were then directly added to the cultures and live fluorescence was monitored in the samples by fluorescent microscopy using a rhodamine filter set (568 nm; Olympus CKX41; Hamburg, Germany) [55,57].

### 2.9.4. Cell Proliferation and Viability

hMSCs were seeded in 24-well plates ( $2 \times 10^4$  cells/well) with growth medium for 12 h at 37 °C under 5% CO<sub>2</sub> prior to direct addition of the PolyCD-based nanoassemblies to the cultures. Cell proliferation was evaluated using the Cell Proliferation Reagent WST-1 according to the manufacturer's recommendations [55–57]. Cell viability was determined with the Cytotoxicity Detection KitPLUS (LDH) in the supernatants of culture by assessing the absorbance at 450 nm on a GENios spectrophotometer/fluorometer (Tecan, Crailsheim, Germany). Cytotoxicity was calculated as follows [57]:

$$\text{cell viability (\%)} = (\text{experimental value} - \text{low control}) / (\text{high control} - \text{low control}) \times 100 \quad (4)$$

### 2.9.5. Inflammatory Responses

hMSCs were seeded in 24-well plates ( $2 \times 10^4$  cells/well) with growth medium for 12 h at 37 °C under 5% CO<sub>2</sub> prior to direct addition of the PolyCD-based nanoassemblies to the cultures. Inflammatory responses were monitored by measuring the production levels of IL-1 $\beta$  and TNF- $\alpha$  in the supernatants of culture by respective ELISAs on a GENios spectrophotometer/fluorometer.

### 2.9.6. Statistical Analysis

All tests were performed in triplicate in three independent experiments. Data are expressed as mean  $\pm$  standard deviation (SD) of separate experiments. The *t*-test was employed where appropriate, with  $p < 0.05$  considered statistically significant.

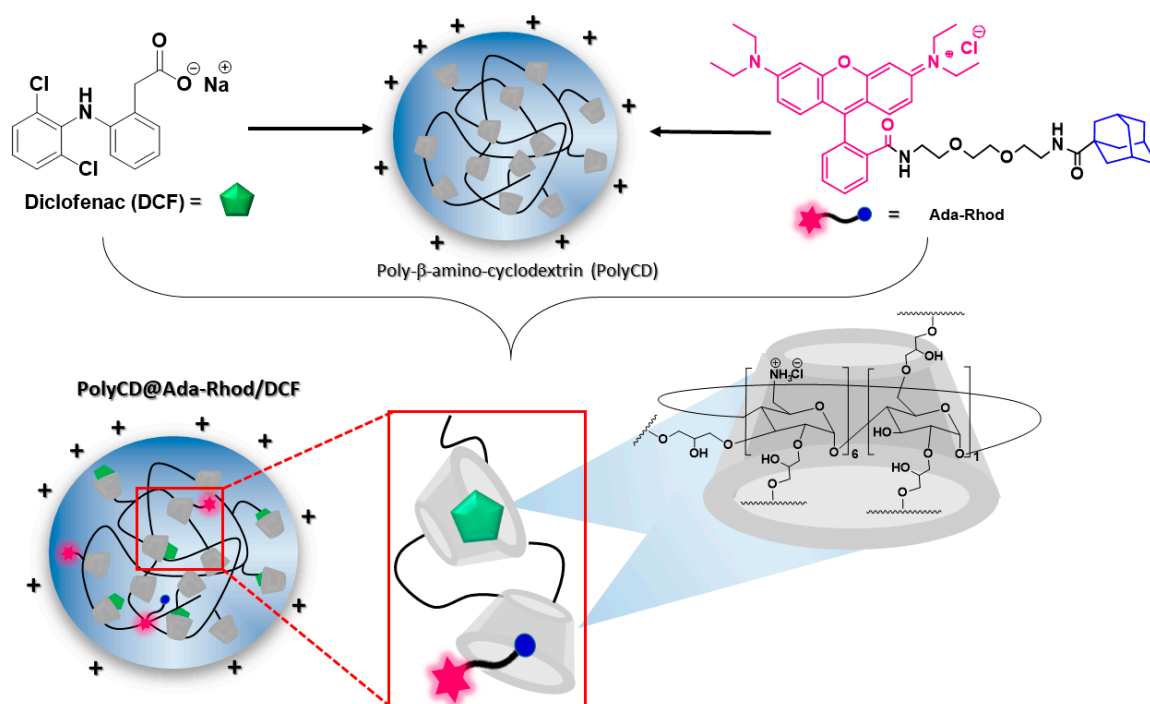
## 3. Results and Discussion

### 3.1. Nanoassemblies Preparation

Fluorescent cationic nanoassemblies entrapping DCF (PolyCD@Ada-Rhod/DCF) were prepared by hydration of Ada-Rhod organic film and the recovered PolyCD@Ada-Rhod was used for the following hydration of DCF organic film. Concentration of CD repetitive units was used in slight excess vs. [DCF], thus to achieve a complete drug entrapment. Scheme 1 summarizes nanoassemblies formation by molecular components.

Nanoassemblies were obtained with high Ada-Rhod and DCF entrapment efficiency ( $\cong 92\%$  and 100%, respectively). Ada-Rhod residual film was used to determine Ada-Rhod loading (see experimental). No residual of DCF was found in the dispersions of PolyCD@Ada-Rhod/DCF, confirming the complete entrapment. Moreover, it was observed that the recovery yield for all systems is 80%, probably because of the presence of a little water percentage in the starting cyclodextrin polymer, due to its highly hygroscopic nature. Properties of nanoassemblies are reported in Table 1.

DLS analysis of PolyCD and PolyCD@AdaRhod/DCF nanoassemblies (Table 1) shows a size distribution centered at a hydrodynamic diameter ( $D_H$ ) of about 250 nm for the main population and a  $\zeta$ -potential of about + 20 mV, due to the positive charges of the amino groups of the polymer network (see Figure S3). Surprisingly PolyCD@AdaRhod showed a size that is about two-fold vs. the analogue with DCF, suggesting a different rearrangement vs. the nanossemblies entrapping both Ada-Rhod and DCF.



**Scheme 1.** Sketched view of nanoassemblies preparation (PolyCD@Ada-Rhod/DCF).

**Table 1.** Overall properties of PolyCD-based nanoassemblies: mean  $D_H$ , polydispersity index (PDI) and  $\zeta$ -potential values ( $\zeta$ ), loading and EE% in ultrapure water.

Sample	Medium	Mean $D_H$ (nm $\pm$ SD) <sup>a</sup>	PDI	$\zeta$ (mV $\pm$ SD)	Theoretical Loading (%)	<sup>c</sup> Actual Loading (%)	<sup>d</sup> EE (%)
PolyCD	H <sub>2</sub> O	268 $\pm$ 10 (97)	0.07	19 $\pm$ 6			
PolyCD@Ada-Rhod	H <sub>2</sub> O	498 $\pm$ 54 (85)	0.2	25 $\pm$ 5	1.28 <sup>(1)</sup>	1.18 $\pm$ 0.04 <sup>(1)</sup>	92.0 $\pm$ 3.3 <sup>(1)</sup>
PolyCD@AdaRhod/DCF	H <sub>2</sub> O	229 $\pm$ 35 (85)	$\leq$ 0.3	22 $\pm$ 4	1.18 <sup>(1)</sup>	1.09 $\pm$ 0.05 <sup>(1)</sup>	92.0 $\pm$ 3.9 <sup>(1)</sup>
					15.5 <sup>(2)</sup>	15.5 <sup>(2)</sup>	$\sim$ 100 <sup>(2)</sup>
	PBS pH 7.4	230 $\pm$ 24 (83)	$\leq$ 0.2				
		25 $\pm$ 13 (11)	$\leq$ 0.2				
	NaCl (0.9 wt %)	228 $\pm$ 21 (89)	$\leq$ 0.2				
		18 $\pm$ 13 (12)					

<sup>a</sup> SD was calculated on three different batches. <sup>b</sup> Mean size with corresponding intensity % distribution (only main populations). <sup>c</sup> Actual loading is expressed as the amount of drug (mg) encapsulated per 100 mg of nanoassembly. <sup>d</sup> Ratio between actual and theoretical loading  $\times$  100. <sup>(1)</sup> Values are referred to Ada-Rhod; <sup>(2)</sup> Values are referred to Diclofenac; PolyCD (0.5 mg/mL) and PolyCD@Ada-Rhod/DCF (0.5 mg/mL, [Ada-Rhod] = 8  $\mu$ M, [DCF] = 236  $\mu$ M).

### 3.2. Interaction Studies and Complexes Formation

The interactions of PolyCD with Ada-Rhod within PolyCD@Ada-Rhod, and with both Ada-Rhod and DCF within PolyCD@Ada-Rhod/DCF were investigated by UV/Vis, steady-state and time-resolved fluorescence emission. PolyCD/DCF complex formation was studied for comparison. UV/Vis spectra and fluorescence emission of free Ada-Rhod in DCM vs. PolyCD@Ada-Rhod complex are shown in Figure 1. Ada-Rhod's absorption profile shows a major band centered at 558 nm in DCM, which was red-shifted at 561 nm in PolyCD@Ada-Rhod. The appearance of absorption profile in water was unambiguous evidence of Ada-Rhod complexation since free Ada-Rhod was not soluble in water (Figure 1A). Steady state emission fluorescence (Figure 1B) of Ada-Rhod in DCM shows a band centered at 575 nm, whereas after the interaction with PolyCD in aqueous medium the emission profile actually split into a band, centered at 542 and a shoulder around 576 nm respectively.

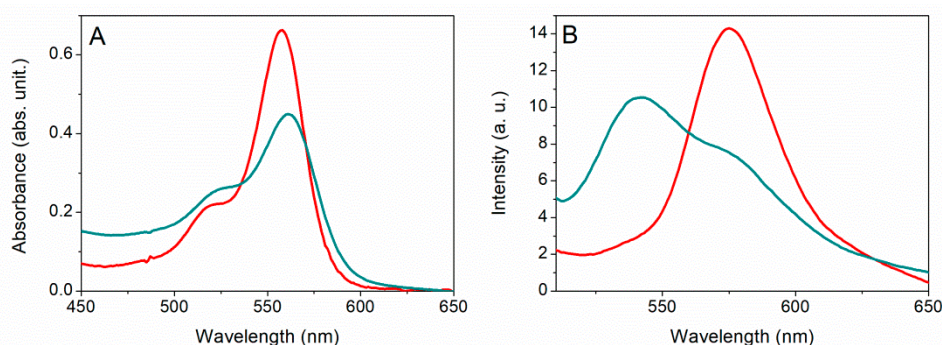


**Figure 1.** UV/Vis spectra (A) and steady state emission spectra (B) of free Ada-Rhod in DCM (red trace) and PolyCD@Ada-Rhod (blue cyan trace) in ultrapure water, pH = 4. (A): 44 mg/mL, [Ada-Rhod] = 713  $\mu$ M, pH = 4, d = 1 cm and scattering subtracted in the spectrum of the PolyCD@Ada-Rhod. (B): 0.5 mg/mL, [Ada-Rhod] = 8  $\mu$ M,  $\lambda_{exc}$  = 480 nm.

This double band profile is typical of rhodamine derivatives because of the tautomeric equilibrium that occurs in water, and is strictly influenced even by slight pH changes in the aqueous microenvironments [58,59].

The interaction of PolyCD with DCF was firstly studied by UV/Vis spectroscopy. The complexation of the drug into PolyCD was obtained by simple mixing of aqueous solutions of DCF and PolyCD as reported in experimental method. The incorporation of DCF into the complex was evident from the UV/Vis spectrum (Figure 2A) that displays a band centered at 276 nm for free DCF (black trace) and 278 nm for the complex in water (orange trace). Furthermore, a slight hyperchromic effect was observed upon complexation. For comparison, a UV/Vis spectrum was recorded on PolyCD/DCF complex obtained by solvent evaporation technique (hydration of organic film and sonication) as reported in the experimental method and the same effect was observed, thus confirming the interaction (Figure S4). Probably the very slight hyperchromicity and shift are due to the excellent dispersibility of both components in water. The stoichiometry of the complex was determined by the continuous variation method [60]. The shape of Job's plot ( $\Delta A/A_0 \times [DCF]$  vs.  $\chi$  DCF) was highly symmetrical, showing a maximum value at  $\chi$  DCF = 0.5 pointing out a formation of complex with prevalent 1:1 stoichiometry (Figure 2B).

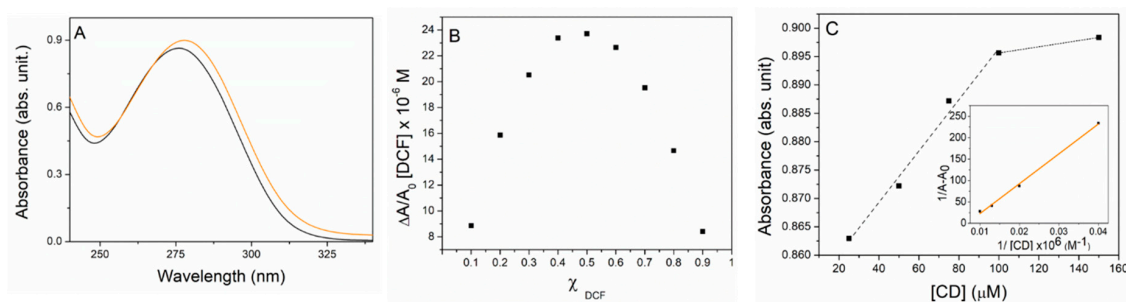


**Figure 2.** (A) UV/Vis spectra of free DCF (black trace) and PolyCD/DCF (orange trace) in water, [CD] = [DCF] = 100  $\mu$ M; (B) Job's plot for the complexation of DCF with PolyCD from UV/Vis measurements in ultrapure water (see Experimental section); and (C) UV/Vis spectral changes of DCF vs. CD concentration (dashed black traces) and plot of  $(1/\Delta A)$  vs.  $1/[CD]$  (inset, orange trace,  $R^2 = 0.997$ ) in ultrapure water, [DCF] = 100  $\mu$ M, [CD] = 25–150  $\mu$ M; d = 1 cm; T = 25  $^{\circ}$ C.

Furthermore, the formation of complex was confirmed by increase of absorbance measured vs. CD concentration in the range 25–150  $\mu$ M. This plot reveals a bimodal behaviour, with a linear increase up to 100  $\mu$ M and afterwards a pseudo plateau (Figure 2C). In the first linear portion a  $A_L$  type diagram with a slope less of a unit was observed. At higher host concentrations complexes with a higher order

and undefined stoichiometry could occur. The apparent binding constant for the 1:1 complex can be evaluated by using the Benesi–Hildebrand Equation [61].

$$\frac{1}{A - A_0} = \frac{1}{K_b \times (A_{\max} - A_0) \times [CD]} + \frac{1}{A_{\max} - A_0} \quad (5)$$

where  $A$  is the absorbance at maximum of the PolyCD/DCF complex,  $A_0$  is the absorbance of DCF in the absence of PolyCD,  $[CD]$  is the PolyCD concentration in CD units,  $A_{\max}$  is the absorbance at  $[CD]_{\max}$  (100  $\mu\text{M}$ ) and  $K_b$  is the apparent binding constant. The apparent binding constant was estimated from the slope  $/(A_{\max} - A_0)$  (plot of  $1/(A - A_0)$  vs.  $1/[CD]$ ) and is found to be  $4.1 \times 10^3 \text{ M}^{-1}$  ( $\log K_b \cong 3.60$ ; inset of Figure 2C). This value agrees with data found for complexation of DCF in cationic CD cross-linked oligomers ( $\log K_b \cong 3.47$ ) [38].

Fluorescence time-decays of Ada-Rhod free and within nanoassemblies were fitted by one and three exponential profiles respectively, estimating three different fluorescence lifetimes when the probe is complexed into the polymeric structure (Table 2 and Figure 3).

**Table 2.** Fluorescence lifetimes ( $\tau$ ) and rotational correlation time ( $\theta_R$ ) of PolyCD@Ada-Rhod/DCF vs. Ada-Rhod.

Sample	$\tau_1 \pm 0.1, \text{ ns}$	$\tau_2 \pm 0.1, \text{ ns}$	$\tau_3 \pm 0.1, \text{ ns}$	$A_1, \%$	$A_2, \%$	$A_3, \%$	$\theta_R \pm 0.2, \text{ ns}$
Ada-Rhod <sup>a</sup>	3.6	–	–	100	–	–	0.8
PolyCD@Ada-Rhod/DCF <sup>a</sup>	0.4	2.4	5.8	23	34	43	2.2

<sup>a</sup> Fluorescence lifetimes were measured at  $\lambda_{\text{exc}} = 390 \text{ nm}$ : Ada-Rhod in DCM,  $\lambda_{\text{em}} = 576 \text{ nm}$ ; PolyCD@Ada-Rhod/DCF in ultrapure water,  $\lambda_{\text{em}} = 576 \text{ nm}$ .  $A$  is the amplitude of the intensity decay. Experimental conditions: free [Ada-Rhod] = 100  $\mu\text{M}$ ; PolyCD@Ada-Rhod/DCF (0.5 mg/mL, [Ada-Rhod] = 8  $\mu\text{M}$ , [DCF] = 236  $\mu\text{M}$ ).

The time fluorescence decay (Figure 3) and correspondent fluorescent lifetimes (Table 2) pointed out that free Ada-Rhod in DCM was present mostly as a monomer ( $\tau_1 = 3.6 \text{ ns}$ ) [62–64]. When analyzing PolyCD@Ada-Rhod/DCF nanoassemblies in ultrapure water, three lifetimes were observed and one of these ( $\tau_2 = 2.4 \text{ ns}$ ) was ascribable to Ada-Rhod species entrapped within the polymer chains in the monomeric form [46,65]. This could also explain the rotational correlation time after interaction of Ada-Rhod within PolyCD@Ada-Rhod/DCF (0.8 ns in free Ada-Rhod vs. 2.2 ns in the nanoassembly), suggesting that the probe is effectively incorporated into the structure, but still maintains a certain freedom to rotate upon itself [51]. For what concerns the shorter lifetimes (0.4 ns in the PolyCD@Ada-Rhod/DCF) it could be supposedly due to self-oligomers formation of Ada-Rhod, likely generated by self  $\pi$ – $\pi$  stacking or other aggregation phenomena that lead to fluorescence quenching. Finally, the longer ones ( $\tau_3 = 5.8 \text{ ns}$ ) were tentatively ascribed to species of Ada-Rhod interacting more closely to CD cavities (i.e., inclusion of Ada portion).

Overall, our investigations indicated that both DCF and Ada-Rhod interact with CD cavities. Host–guest complexation of Ada-Rhod takes advantage of the high affinity of adamantane portion for CD cavities ( $K_b = 5 \times 10^4 \text{ M}^{-1}$ ) [66], and this interaction is stronger with respect to DCF with a CD cavity: indeed no Ada-Rhod displacement was observed even if DCF was used in excess vs. Ada-Rhod. The formation of larger aggregates in PolyCD@Ada-Rhod rather than PolyCD@Ada-Rhod/DCF is an experimental evidence that was already observed in others nanoassemblies based on polymeric systems functionalized with rhodamine [67]. We suppose that upon inclusion of the adamantane unit into CD cavity, the rhodamine residue of Ada-Rhod is located in a more hydrophilic environment, likely outside the CD cavity and in the proximity of the CD rims. Moreover, the formation of supramolecular self-oligomers of Ada-Rhod with shorter fluorescence lifetimes (0.4 ns with amplitude of 23%) could occur. These arrangements could allow in average an increase of  $D_H$  (see Table 1) in PolyCD@Ada-Rhod. On the other hand, the decrease of  $D_H$  and  $\zeta$ -potential values in PolyCD@Ada-Rhod/DCF could be tentatively ascribed to the formation of more compacted and smaller nanoassemblies due to an

increased colloidal stability originated from the significant interactions of DCF with both CD cavity and cationic external CD rims, as clearly indicated by UV-Vis, DLS and  $\zeta$ -potential results.

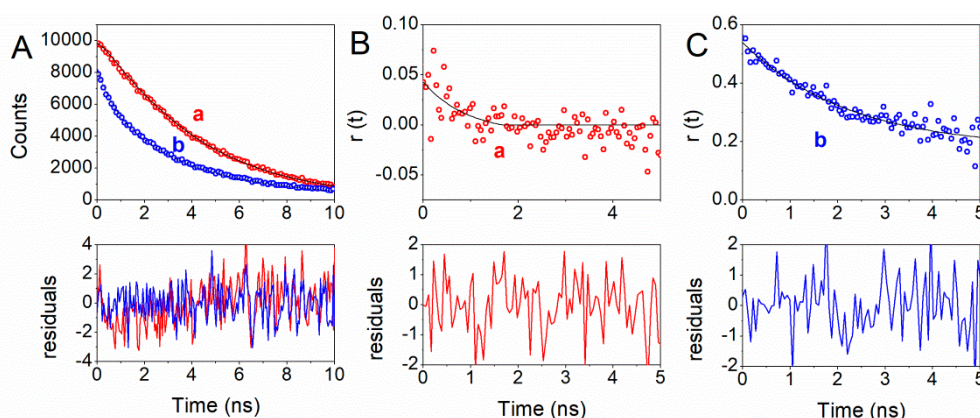


**Figure 3.** Fluorescence time decay (A) and time-resolved fluorescence anisotropy (B,C) of a) Ada-Rhod 100  $\mu$ M in DCM and b) PolyCD@Ada-Rhod/DCF (0.5 mg/mL, [Ada-Rhod] = 8  $\mu$ M, [DCF] = 236  $\mu$ M) in ultrapure water at room temperature (r.t.).

### 3.3. Stability and Release Studies

In order to investigate if the aggregation properties of the nanoassemblies are influenced by a dispersing medium, we carried out stability studies vs. time in ultrapure water and in biologically relevant media by DLS and UV/Vis. For freshly prepared solutions at  $t = 0$ , the UV/Vis profile of DCF within PolyCD@Ada-Rhod/DCF showed the band centered at 278 nm. The changes of absorption spectra,  $D_H$  and  $\zeta$ -potential vs. time for PolyCD@Ada-Rhod/DCF nanoassemblies in ultrapure water are shown in Figure 4. Within two weeks, the absorbance of the band at 278 nm decreased about 30% with respect to the freshly prepared dispersion. Size of the nanoassemblies was monitored for up to 2 weeks. At  $t = 0$ , all the samples exhibited a size distribution with a mean diameter roughly of 250 nm, which remains approximately constant for the first 7 days. The  $\zeta$ -potential values vs. time were measured in ultrapure water at r.t. With a starting value at  $t = 0$  around 20 mV, a significant decrease was observed from the 7th day on. However, the sharply positive surface charge is advantageous for a rapid cellular uptake of the nanoassemblies from the target cells, which should be completed far before one week from the local administration.

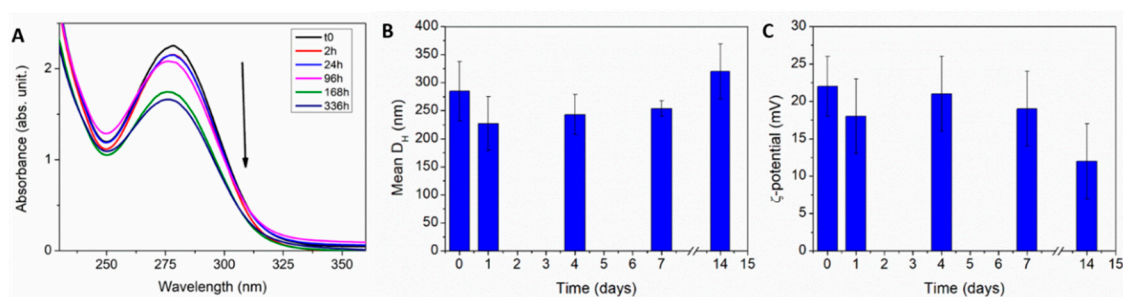


**Figure 4.** UV/Vis spectra (A), mean  $D_H$  (main populations only) (B) and  $\zeta$ -potential (C) vs. time of PolyCD@Ada-Rhod/DCF nanoassemblies in ultrapure water (0.5 mg/mL, [Ada-Rhod] = 8  $\mu$ M, [DCF] = 236  $\mu$ M). Data were acquired at  $t = 0, 1, 4, 7$  and 14 days. Nanoassemblies dispersions were stored at 25  $^{\circ}$ C under stirring along the experimental time.

As far as it concerns the other biological media (PBS and NaCl 0.9 wt %), an immediate increase in size was observable after the first day (see Figures S5 and S6), suggesting that the aggregation

properties of the nanoassemblies can be influenced by the medium ionic strength. After 2 weeks, the size significantly increased for all the dispersions in all media.

In conclusion, it is possible to assess that PolyCD@Ada-Rhod/DCF nanoassemblies were stable in aqueous medium at 25 °C up to 7 days. On the contrary, it is advisable to administer the saline injectable formulation within the first day after reconstitution, for maintaining a high concentration of DCF loaded in the nanoformulation. This expedient could allow in view of the potential application of these nanosystems to further prolong and sustain their performance in the joint [68–70].

Kinetic release profiles of DCF from PolyCD@Ada-Rhod/DCF were evaluated in PBS at 37 °C up to 10 days (Figure 5). Released DCF was determined using the calibration curve by UV/Vis of DCF in PBS (Figure S2B). No initial burst release was observed from the nanoassembly, with a slow and controlled release in time, leading to a final 35% of DCF in the external medium. The corresponding unreleased amount of drug in the donor compartment (60%) was determined by UV/Vis analysis.

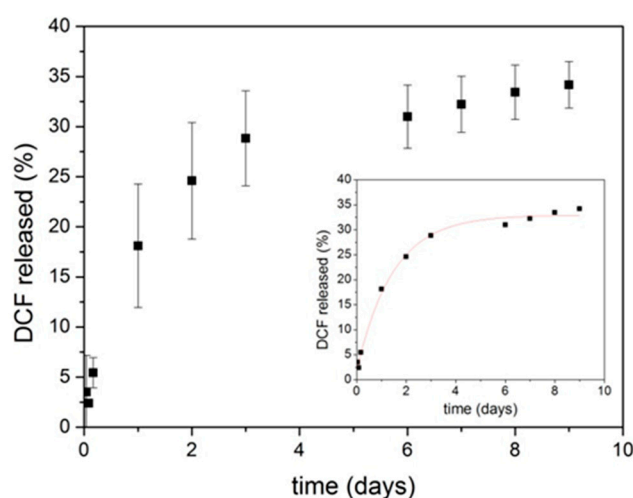


**Figure 5.** Release profile of DCF from PolyCD@Ada-Rhod/DCF nanoassemblies in PBS (pH = 7.4) at 37 °C (Spectra/Por®dialysis bags, MWCO 3.5 kDa). Data are reported as the mean three independent experiments ± SD. In the inset experimental data are best-fitted first order kinetic model.

The kinetic analysis was carried out by three different models reported in the literature by Higuchi, Baker–Lonsdale and a simple first order process for different pharmaceutical dosage forms (i.e., semisolid and solid; see Table 3 and SI) [54,71] and potentially applicable to nanoparticulate dispersions [53,72].

**Table 3.** Regression coefficient ( $R^2$ ) and rate constants ( $k_H$  and  $k$ ) of DCF release data from PolyCD@Ada-Rhod/DCF fitted according to different kinetic models.

Higuchi		Baker-Lonsdale		First order	
$R^2$	$k_H$ ( $h^{-1/2}$ )	$R^2$	$k$ ( $h^{-1}$ )	$R^2$	$k$ ( $h^{-1}$ )
0.9047	$12.8057 \pm 0.6679$	0.9241	$3.3 \times 10^{-3} \pm 3 \times 10^{-4}$	0.9952	$0.6828 \pm 0.0552$

By best-fit of data (inset of Figure 5) it was possible to evaluate the regression coefficient ( $R^2$ ) and release parameters ( $k/h^{-1}$ ). By considering a first order process, as commonly known for molecular permeation across a membrane from a stirred donor into a stirred receiving phase under quasi-stationary and sink conditions [73], the model can be represented by the following Equation:

$$C_t = C_\infty(1 - e^{-kt}) \quad (6)$$

where  $C_t$  and  $C_\infty$  are the amount of drug released (in percentage) in the receiving phase at time  $t$  and at  $t_\infty$ , at the end of release process, and  $k$  is the rate constant of the process. Altogether, kinetic analysis agrees with a simple monoexponential decay that is the release of DCF from the nanoassembly is a dependent first order process, showing a plateau of drug released ( $\cong 36\%$ ) after about 10 days.

### 3.4. Biological Studies

#### 3.4.1. Effective Targeting of hMSCs with PolyCD-based Nanoassemblies

hMSCs were treated with PolyCD-based nanoassemblies in order to examine their ability to deliver DCF. A strong fluorescent signal was detected in hMSCs receiving PolyCD@Ada-Rhod/DCF already after 2 h of incubation and for at least 24 h compared with the control conditions (positive control: PolyCD@Ada-Rhod in absence of DCF; negative controls: DCF alone, DMEM; Figure 6).

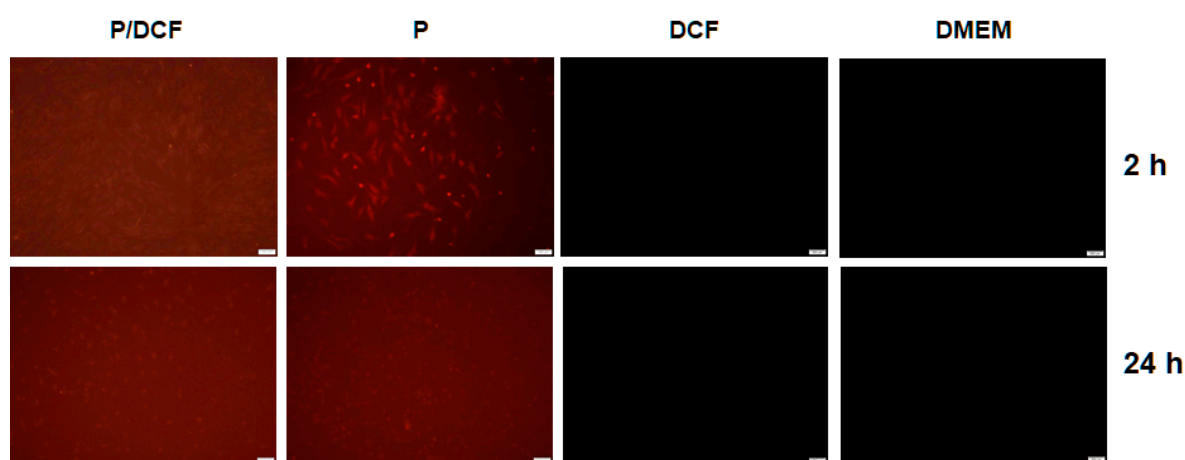


**Figure 6.** Detection of live fluorescence in human mesenchymal stromal cells (hMSCs) treated with PolyCD-based nanoassemblies (2 mg/mL). hMSCs ( $2 \times 10^4$  cells/well in 24-well plates) were directly incubated with the compounds and live fluorescence was monitored after 2 and 24 h by fluorescent microscopy as described in the Materials and Methods (scale bars: 200  $\mu\text{m}$ ). Abbreviations: P/DCF: PolyCD@Ada-Rhod/DCF; P: PolyCD@Ada-Rhod. DMEM: Dulbecco's modified Eagle's medium.

#### 3.4.2. Cell Proliferation and Viability of hMSCs Treated with the PolyCD-based Nanoassemblies

PolyCD-based nanoassemblies were next applied to the hMSCs to evaluate their potential deleterious effects on the levels of cell proliferation and viability. Importantly, no detrimental effects of the PolyCD@Ada-Rhod/DCF treatment relative to all other control conditions (PolyCD@Ada-Rhod in the absence of DCF, DCF alone and DMEM) were observed after 48 h on the cell proliferation indices ( $p \geq 0.087$ ; Figure 7A) or on the percent of cell viability ( $p \geq 0.081$ ; Figure 7B).

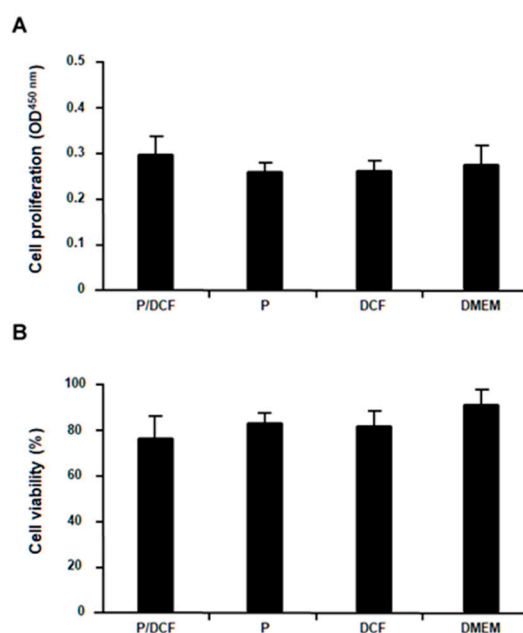


**Figure 7.** Analysis of cell proliferation and viability of hMSCs treated with the PolyCD-based nanoassemblies (2 mg/mL). hMSCs ( $2 \times 10^4$  cells/well in 24-well plates) were directly incubated with the compounds. Cell proliferation was evaluated using the Cell Proliferation Reagent WST-1 (A) and cell viability with the Cytotoxicity Detection KitPLUS (LDH) (B) after 48 h. Abbreviations: P/DCF: PolyCD@Ada-Rhod/DCF; P: PolyCD@Ada-Rhod.

### 3.4.3. Protective Effects of DCF Treatment Against Inflammation in hMSCs Treated with PolyCD-based Nanoassemblies

PolyCD@Ada-Rhod/DCF was finally provided to hMSCs to evidence possible protective activities of the system against proinflammatory responses. Remarkably, the intrinsic levels of IL-1 $\beta$  production in hMSCs were significantly reduced after 48 h in the presence of PolyCD@Ada-Rhod/DCF versus all other conditions (PolyCD@Ada-Rhod in absence of DCF, DCF alone, DMEM; up to 1.6-fold decrease,  $p \leq 0.002$ ; Figure 8A). Application of DCF alone also displayed a protective effect against IL-1 $\beta$  production relative to PolyCD@Ada-Rhod (without DCF) and DMEM but to a lesser extent than when provided via the PolyCD compound (up to 1.1-fold decrease,  $p \leq 0.040$ ; Figure 8A). The intrinsic levels of TNF- $\alpha$  production in hMSCs were also significantly reduced after 48 h in the presence of PolyCD@Ada-Rhod/DCF versus PolyCD@Ada-Rhod (without DCF) and DMEM (up to 1.2-fold decrease,  $p \leq 0.003$ ), but without significant difference relative to DCF alone ( $p = 0.188$ ) that also had a protective effect against TNF- $\alpha$  production versus PolyCD@Ada-Rhod (without DCF) and DMEM (up to 1.1-fold decrease,  $p \leq 0.001$ ; Figure 8B).

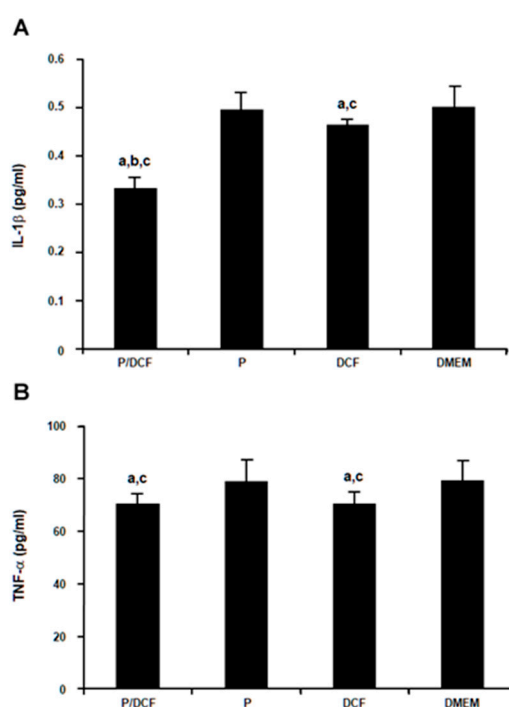


**Figure 8.** Analysis of inflammatory responses in hMSCs treated with PolyCD-based nanoassemblies (2 mg/mL). hMSCs ( $2 \times 10^4$  cells/well in 24-well plates) were directly incubated with the compounds. Inflammatory responses (**A**: IL-1 $\beta$ ; **B**: TNF $\alpha$ ) were detected using IL-1 $\beta$  and TNF- $\alpha$  ELISAs, respectively, after 48 h as described in the Materials and Methods. Statistically significant compared with DMEM (a), DCF (b), and P (c). Abbreviations: P/DCF: PolyCD@Ada-Rhod/DCF; P: PolyCD@Ada-Rhod.

#### 4. Conclusions

In summary, the present work shows the possibility to develop fluorescently labeled PolyCD-based nanoassemblies entrapping the non-steroidal anti-inflammatory drug diclofenac (DCF) as therapeutic, anti-inflammatory nanomedicines to tackle critical pathological inflammation in OA. PolyCD was selected to take advantage of its intrinsic capability to encapsulate a wide variety of active agents and to regulate the release mechanisms by exploiting the affinity constant of the polymer for complexed guests and their hydrophilic/lipophilic features. In this study, we exploited PolyCD as a suitable theranostic platform with simultaneous loading of the therapeutic agent DCF and of the fluorescent probe Ada-Rhod. The elucidation of the PolyCD@Ada-Rhod/DCF physicochemical properties, such as size, surface charges and stability in biologically relevant media, release, etc., suggested the adequacy of PolyCD-based nanoassemblies for intra-articular delivery strategies. PolyCD-based nanoassemblies were stable in aqueous medium at 25 °C for up to 7 days and one day in saline injectable formulation after reconstitution. Release experiments evidenced a different aptitude to deliver the payloads: a retarded release without burst effect (with a plateau of released DCF ( $\approx 35\%$ , after about 10 days) was found for DCF, whereas no trace of fluorescent probe (Ada-Rhod) was detected in the aqueous medium. In the particular case of the intra-articular delivery, the size and zeta potential of the polyCD@Ada-Rhod/DCF appeared suitable to develop a syringeable formulation that could sustainably release the anti-inflammatory drug for several weeks at the site of injection, allowing for a localized treatment. Importantly, the results of the biological evaluations revealed no detrimental effects of PolyCD@Ada-Rhod/DCF on cell proliferation and viability in hMSCs and a fast cellular uptake (within 2 h) in the cells that remained fluorescent until 24 h. Finally, the data demonstrated the significant anti-inflammatory potential of PolyCD@Ada-Rhod/DCF against the production of IL-1 $\beta$  in hMSCs *in vitro*, as a promising future tool to contain inflammatory pathomechanisms in OA.

**Supplementary Materials:** The following are available online at <http://www.mdpi.com/2079-4991/10/9/1712/s1>: 1. Estimation of CD cavities in PolyCD and amino groups content; 2. Analysis of release kinetic; Figure S1: Lambert-Beer of free Ada-Rhod in DCM; Figure S2: Lambert-Beer of free DCF in ultrapure water and PBS; Figure S3: Size (or  $D_H$ ) distribution of PolyCD (black line) and PolyCD@Ada-Rhod/DCF; Figure S4: UV/Vis of free DCF and PolyCD/DCF in ultrapure water obtained by solvent evaporation technique; Figure S5: Stability studies of PolyCD@Ada-Rhod/DCF in NaCl wt. 0.9%; Figure S6: Stability studies of PolyCD@Ada-Rhod/DCF in PBS.

**Author Contributions:** Conceptualization A.P. and A.M.; investigation, A.C., R.Z., M.M. and J.K.V.; data curation, A.C., M.C.; A.P.; A.M., writing—original draft preparation, A.C., M.C., A.P. and A.M. writing—review and editing, C.A.-L., M.C., A.P. and A.M.; visualization, A.C., R.Z., J.K.V.; Supervision, A.M. All authors discussed the results and commented on the manuscript. All authors have read and agreed to the published version of the manuscript.

**Funding:** This research was funded by MaTisse (CNR-ISMN Project 4, A. P. 11/2017, Sicily Region, FSE 2014/2020) and PON03PE\_00216\_1 Drug Delivery.

**Conflicts of Interest:** The authors declare no conflict of interest.

## References

1. Hawker, G.A.; Stanaitis, I. Osteoarthritis year in review 2014: Clinical. *Osteoarthr. Cartil.* **2014**, *22*, 1953–1957. [[CrossRef](#)] [[PubMed](#)]
2. Goldring, M.B.; Goldring, S.R. Osteoarthritis. *J. Cell Physiol.* **2007**, *213*, 626–634. [[CrossRef](#)] [[PubMed](#)]
3. Madry, H.; Grün, U.W.; Knutsen, G. Cartilage repair and joint preservation: Medical and surgical treatment options. *Dtsch. Arztebl. Int.* **2011**, *108*, 669–677. [[CrossRef](#)] [[PubMed](#)]
4. Madry, H.; Cucchiaroni, M. Gene therapy for human osteoarthritis: Principles and clinical translation. *Expert Opin. Biol. Ther.* **2016**, *16*, 331–346. [[CrossRef](#)] [[PubMed](#)]
5. Geiger, B.C.; Grodzinsky, A.J.; Hammond, P.T. Designing Drug Delivery Systems for Articular Joints. *Chem. Eng. Prog.* **2018**, *114*, 46–51.
6. Rivera-Delgado, E.; Djuhadi, A.; Danda, C.; Kenyon, J.; Maia, J.; Caplan, A.I.; von Recum, H.A. Injectable liquid polymers extend the delivery of corticosteroids for the treatment of osteoarthritis. *J. Control Release* **2018**, *284*, 112–121. [[CrossRef](#)]
7. Shah, N.J.; Geiger, B.C.; Quadir, M.A.; Hyder, N.; Krishnan, Y.; Grodzinsky, A.J.; Hammond, P.T. Synthetic nanoscale electrostatic particles as growth factor carriers for cartilage repair. *Bioeng. Transl. Med.* **2016**, *1*, 347–356. [[CrossRef](#)]
8. Dong, R.; Pang, Y.; Su, Y.; Zhu, X. Supramolecular hydrogels: Synthesis, properties and their biomedical applications. *Biomater. Sci.* **2015**, *3*, 937–954. [[CrossRef](#)]
9. Crini, G. Review: A history of cyclodextrins. *Chem Rev.* **2014**, *114*, 10940–10975. [[CrossRef](#)]
10. Hu, Y.; Li, Y.; Xu, F.J. Versatile Functionalization of Polysaccharides via Polymer Grafts: From Design to Biomedical Applications. *Acc. Chem. Res.* **2017**, *50*, 281–292. [[CrossRef](#)]
11. Folch-Cano, C.; Yazdani-Pedram, M.; Olea-Azar, C. Inclusion and functionalization of polymers with cyclodextrins: Current applications and future prospects. *Molecules* **2014**, *19*, 14066–14079. [[CrossRef](#)] [[PubMed](#)]
12. Nielsen, A.L.; Steffensen, K.; Larsen, K.L. Self-assembling microparticles with controllable disruption properties based on cyclodextrin interactions. *Colloids Surf. B Biointerfaces* **2009**, *73*, 267–275. [[CrossRef](#)] [[PubMed](#)]
13. Xiong, Q.; Cui, M.; Bai, Y.; Liu, Y.; Liu, D.; Song, T. A supramolecular nanoparticle system based on beta-cyclodextrin-conjugated poly-l-lysine and hyaluronic acid for co-delivery of gene and chemotherapy agent targeting hepatocellular carcinoma. *Colloids Surf. B Biointerfaces* **2017**, *155*, 93–103. [[CrossRef](#)] [[PubMed](#)]
14. Zhang, Y.; Jiang, Q.; Wojnilowicz, M.; Pan, S.; Ju, Y.; Zhang, W.; Liu, J.; Zhuo, R.; Jiang, X. Acid-sensitive poly( $\beta$ -cyclodextrin)-based multifunctional supramolecular gene vector. *Polym. Chem.* **2018**, *9*, 450–462. [[CrossRef](#)]
15. Fülöp, Z.; Kurkov, S.; Nielsen, T.; Larsen, K.L.; Loftsson, T. Self-assembly of cyclodextrins: Formation of cyclodextrin polymer based nanoparticles. *J. Drug Deliv. Sci. Technol.* **2012**, *22*, 215–221. [[CrossRef](#)]
16. Layre, A.-M.; Volet, G.; Wintgens, V.; Amiel, C. Associative Network Based on Cyclodextrin Polymer: A Model System for Drug Delivery. *Biomacromolecules* **2009**, *10*, 3283–3289. [[CrossRef](#)]

17. Othman, M.; Bouchemal, K.; Couvreur, P.; Desmaële, D.; Morvan, E.; Pouget, T.; Gref, R. A comprehensive study of the spontaneous formation of nanoassemblies in water by a “lock-and-key” interaction between two associative polymers. *J. Colloid Interfaces Sci.* **2011**, *354*, 517–527. [[CrossRef](#)]
18. Trotta, F.; Zanetti, M.; Cavalli, R. Cyclodextrin-based nanosponges as drug carriers. *Beilstein J. Org. Chem.* **2012**, *8*, 2091–2099. [[CrossRef](#)]
19. Grumezescu, A.M. *Organic Materials as Smart Nanocarriers for Drug Delivery*, 1st ed.; Andrew, W., Ed.; Elsevier: Norwich, NY, USA, 2018. [[CrossRef](#)]
20. Osmani, R.A.; Kulkarni, P.; Manjunatha, S.; Vaghela, R.; Bhosale, R. Cyclodextrin nanosponge-based systems in drug delivery and nanotherapeutics: Current progress and future prospects. In *Organic Materials as Smart Nanocarriers for Drug Delivery*; Grumezescu, A.M., Ed.; William Andrew Publishing: Norwich, NY, USA, 2018; pp. 659–717. [[CrossRef](#)]
21. Gidwani, B.; Vyas, A.J.C.; Biointerfaces, S.B. Synthesis, characterization and application of epichlorohydrin- $\beta$ -cyclodextrin polymer. *Colloids Surf. B Biointerfaces* **2014**, *114*, 130–137. [[CrossRef](#)]
22. Anand, R.; Manoli, F.; Manet, I.; Daoud-Mahammed, S.; Agostoni, V.; Gref, R.; Monti, S.  $\beta$ -Cyclodextrin polymer nanoparticles as carriers for doxorubicin and artemisinin: A spectroscopic and photophysical study. *Photochem. Photobiol. Sci.* **2012**, *11*, 1285–1292. [[CrossRef](#)]
23. Malanga, M.; Seggio, M.; Kirejev, V.; Fraix, A.; Di Bari, I.; Fenyvesi, E.; Ericson, M.B.; Sortino, S. A phototherapeutic fluorescent  $\beta$ -cyclodextrin branched polymer delivering nitric oxide. *Biomater. Sci.* **2019**, *7*, 2272–2276. [[CrossRef](#)] [[PubMed](#)]
24. He, C.; Guo, D.; Chen, K.; Wang, S.; Shen, J.; Zhao, N.; Liu, A.; Zheng, Y.; Li, P.; Wu, Z.; et al.  $\alpha$ -Ga<sub>2</sub>O<sub>3</sub> Nanorod Array–Cu<sub>2</sub>O Microsphere p–n Junctions for Self-Powered Spectrum-Distinguishable Photodetectors. *ACS Appl. Nano Mater.* **2019**, *2*, 4095–4103. [[CrossRef](#)]
25. Castriciano, M.A.; Zagami, R.; Casaletto, M.P.; Martel, B.; Trapani, M.; Romeo, A.; Villari, V.; Sciortino, M.T.; Grasso, L.; Guglielmino, S.; et al. Poly(carboxylic acid)-Cyclodextrin/Anionic Porphyrin Finished Fabrics as Photosensitizer Releasers for Antimicrobial Photodynamic Therapy. *Biomacromolecules* **2017**, *18*, 1134–1144. [[CrossRef](#)]
26. Sobocinski, J.; Laure, W.; Taha, M.; Courcot, E.; Chai, F.; Simon, N.; Addad, A.; Martel, B.; Haulon, S.; Woisel, P.; et al. Mussel Inspired Coating of a Biocompatible Cyclodextrin Based Polymer onto CoCr Vascular Stents. *Acs Appl. Mater. Interfaces* **2014**, *6*, 3575–3586. [[CrossRef](#)]
27. Kersani, D.; Mougin, J.; Lopez, M.; Degoutin, S.; Tabary, N.; Cazaux, F.; Janus, L.; Maton, M.; Chai, F.; Sobocinski, J.; et al. Stent coating by electrospinning with chitosan/poly-cyclodextrin based nanofibers loaded with simvastatin for restenosis prevention. *Eur. J. Pharm. Biopharm.* **2020**, *150*, 156–167. [[CrossRef](#)]
28. Gil, E.S.; Li, J.; Xiao, H.; Lowe, T.L. Quaternary Ammonium  $\beta$ -Cyclodextrin Nanoparticles for Enhancing Doxorubicin Permeability across the In Vitro Blood–Brain Barrier. *Biomacromolecules* **2009**, *10*, 505–516. [[CrossRef](#)]
29. Belbekhouche, S.; Oniszczuk, J.; Pawlak, A.; El Joukhar, I.; Goffin, A.; Varrault, G.; Sahali, D.; Carbonnier, B. Cationic poly(cyclodextrin)/alginate nanocapsules: From design to application as efficient delivery vehicle of 4-hydroxy tamoxifen to podocyte in vitro. *Colloids Surf. B Biointerfaces* **2019**, *179*, 128–135. [[CrossRef](#)]
30. Soltani, Y.; Goodarzi, N.; Mahjub, R. Preparation and characterization of self nano-emulsifying drug delivery system (SNEDDS) for oral delivery of heparin using hydrophobic complexation by cationic polymer of  $\beta$ -cyclodextrin. *Drug Dev. Ind. Pharm.* **2017**, *43*, 1899–1907. [[CrossRef](#)]
31. Thomsen, H.; Benkovics, G.; Fenyvesi, É.; Farewell, A.; Malanga, M.; Ericson, M.B. Delivery of cyclodextrin polymers to bacterial biofilms—An exploratory study using rhodamine labelled cyclodextrins and multiphoton microscopy. *Int. J. Pharm.* **2017**, *531*, 650–657. [[CrossRef](#)]
32. Iohara, D.; Okubo, M.; Anraku, M.; Uramatsu, S.; Shimamoto, T.; Uekama, K.; Hirayama, F. Hydrophobically Modified Polymer/ $\alpha$ -Cyclodextrin Thermoresponsive Hydrogels for Use in Ocular Drug Delivery. *Mol. Pharm.* **2017**, *14*, 2740–2748. [[CrossRef](#)]
33. Scavone, C.; Bonagura, A.C.; Fiorentino, S.; Cimmaruta, D.; Cenami, R.; Torella, M.; Fossati, T.; Rossi, F. Efficacy and Safety Profile of Diclofenac/Cyclodextrin and Progesterone/Cyclodextrin Formulations: A Review of the Literature Data. *Drugs RD* **2016**, *16*, 129–140. [[CrossRef](#)]
34. Mehta, S.K.; Bhasin, K.K.; Dham, S. Energetically favorable interactions between diclofenac sodium and cyclodextrin molecules in aqueous media. *J. Colloid Interface Sci.* **2008**, *326*, 374–381. [[CrossRef](#)]

35. Bogdan, M.; Caira, M.R.; Bogdan, D.; Morari, C.; Fărcaș, S.I. Evidence of a Bimodal Binding between Diclofenac-Na and  $\beta$ -Cyclodextrin in Solution. *J. Incl. Phenom. Macrocycl. Chem.* **2004**, *49*, 225–229. [[CrossRef](#)]
36. Abdoh, A.; Zughul, M.; Davies, J.E.D.; Badwan, A. Inclusion complexation of diclofenac with natural and modified cyclodextrins explored through phase solubility, <sup>1</sup>H-NMR and molecular modeling studies. *J. Incl. Phenom.* **2007**, *57*, 503–510. [[CrossRef](#)]
37. Das, S.; Subuddhi, U. Studies on the complexation of diclofenac sodium with  $\beta$ -cyclodextrin: Influence of method of preparation. *J. Mol. Struct.* **2015**, *1099*, 482–489. [[CrossRef](#)]
38. Giglio, V.; Sgarlata, C.; Vecchio, G. Novel amino-cyclodextrin cross-linked oligomer as efficient carrier for anionic drugs: A spectroscopic and nanocalorimetric investigation. *RSC Adv.* **2015**, *5*, 16664–16671. [[CrossRef](#)]
39. Shi, L.-B.; Tang, P.-F.; Zhang, W.; Zhao, Y.-P.; Zhang, L.-C.; Zhang, H. Aceclofenac-Hydroxypropyl- $\beta$ -Cyclodextrin Complex for Prolonged and Improved Drug Delivery for Orthopedic Applications. *J. Biomater. Tissue Eng.* **2017**, *7*, 327–332. [[CrossRef](#)]
40. Zagami, R.; Mazzaglia, A.; Romeo, A. Bio-soft cyclodextrin nanomaterials. *Riv. Nuovo Cim.* **2019**, *42*, 407–441. [[CrossRef](#)]
41. Bariguan Revel, F.; Fayet, M.; Hagen, M. Topical Diclofenac, an Efficacious Treatment for Osteoarthritis: A Narrative Review. *Rheumatol. Ther.* **2020**, *7*, 217–236. [[CrossRef](#)]
42. Zhou, H.-f.; Yan, H.; Senpan, A.; Wickline, S.A.; Pan, D.; Lanza, G.M.; Pham, C.T.N. Suppression of inflammation in a mouse model of rheumatoid arthritis using targeted lipase-labile fumagillin prodrug nanoparticles. *Biomaterials* **2012**, *33*, 8632–8640. [[CrossRef](#)]
43. Rey-Rico, A.; Babicz, H.; Madry, H.; Concheiro, A.; Alvarez-Lorenzo, C.; Cucchiari, M. Supramolecular polypseudorotaxane gels for controlled delivery of rAAV vectors in human mesenchymal stem cells for regenerative medicine. *Int. J. Pharm.* **2017**, *531*, 492–503. [[CrossRef](#)] [[PubMed](#)]
44. Rey-Rico, A.; Cucchiari, M. Supramolecular Cyclodextrin-Based Hydrogels for Controlled Gene Delivery. *Polymers* **2019**, *11*, 514. [[CrossRef](#)] [[PubMed](#)]
45. Malanga, M.; Bálint, M.; Puskás, I.; Tuza, K.; Sohajda, T.; Jicsinszky, L.; Sente, L.; Fenyvesi, É. Synthetic strategies for the fluorescent labeling of epichlorohydrin-branched cyclodextrin polymers. *Beilstein J. Org. Chem.* **2014**, *10*, 3007–3018. [[CrossRef](#)] [[PubMed](#)]
46. Piperno, A.; Mazzaglia, A.; Scala, A.; Pennisi, R.; Zagami, R.; Neri, G.; Torcasio, S.M.; Rosmini, C.; Mineo, P.G.; Potara, M.; et al. Casting Light on Intracellular Tracking of a New Functional Graphene-Based MicroRNA Delivery System by FLIM and Raman Imaging. *ACS Appl. Mater. Interfaces* **2019**, *11*, 46101–46111. [[CrossRef](#)]
47. Kauscher, U.; Stuart, M.C.A.; Drücker, P.; Galla, H.-J.; Ravoo, B.J. Incorporation of Amphiphilic Cyclodextrins into Liposomes as Artificial Receptor Units. *Langmuir* **2013**, *29*, 7377–7383. [[CrossRef](#)]
48. Kaiser, E.; Colescott, R.L.; Bossinger, C.D.; Cook, P.I. Color test for detection of free terminal amino groups in the solid-phase synthesis of peptides. *Anal. Biochem.* **1970**, *34*, 595–598. [[CrossRef](#)]
49. Tuci, G.; Vinattieri, C.; Luconi, L.; Ceppatelli, M.; Cicchi, S.; Brandi, A.; Filippi, J.; Melucci, M.; Giambastiani, G. “Click” on tubes: A versatile approach towards multimodal functionalization of SWCNTs. *Chemistry* **2012**, *18*, 8454–8463. [[CrossRef](#)]
50. Zagami, R.; Sortino, G.; Caruso, E.; Malacarne, M.C.; Banfi, S.; Patanè, S.; Monsù Scolaro, L.; Mazzaglia, A. Tailored-BODIPY/Amphiphilic Cyclodextrin Nanoassemblies with PDT Effectiveness. *Langmuir* **2018**, *34*, 8639–8651. [[CrossRef](#)]
51. Maiti, N.C.; Krishna, M.M.G.; Britto, P.J.; Periasamy, N. Fluorescence Dynamics of Dye Probes in Micelles. *J. Phys. Chem. B* **1997**, *101*, 11051–11060. [[CrossRef](#)]
52. Gidwani, B.; Vyas, A.; Deep Kaur, C. Investigation of inclusion behaviour of gefitinib with epichlorohydrin- $\beta$ -cyclodextrin polymer: Preparation of binary complex, stoichiometric determination and characterization. *J. Pharm. Biomed. Anal.* **2018**, *160*, 31–37. [[CrossRef](#)]
53. Zagami, R.; Franco, D.; Pipkin, J.D.; Antle, V.; De Plano, L.; Patanè, S.; Guglielmino, S.; Monsù Scolaro, L.; Mazzaglia, A. Sulfobutylether- $\beta$ -cyclodextrin/5,10,15,20-tetrakis(1-methylpyridinium-4-yl)porphine nanoassemblies with sustained antimicrobial phototherapeutic action. *Int. J. Pharm.* **2020**, *585*, 119487. [[CrossRef](#)] [[PubMed](#)]

54. Siepmann, J.; Peppas, N.A. Higuchi equation: Derivation, applications, use and misuse. *Int. J. Pharm.* **2011**, *418*, 6–12. [[CrossRef](#)] [[PubMed](#)]
55. Cucchiari, M.; Ekici, M.; Schetting, S.; Kohn, D.; Madry, H. Metabolic activities and chondrogenic differentiation of human mesenchymal stem cells following recombinant adeno-associated virus-mediated gene transfer and overexpression of fibroblast growth factor 2. *Tissue Eng. Part A* **2011**, *17*, 1921–1933. [[CrossRef](#)] [[PubMed](#)]
56. Venkatesan, J.K.; Ekici, M.; Madry, H.; Schmitt, G.; Kohn, D.; Cucchiari, M. SOX9 gene transfer via safe, stable, replication-defective recombinant adeno-associated virus vectors as a novel, powerful tool to enhance the chondrogenic potential of human mesenchymal stem cells. *Stem Cell Res. Ther.* **2012**, *3*, 22. [[CrossRef](#)] [[PubMed](#)]
57. Rey-Rico, A.; Venkatesan, J.K.; Schmitt, G.; Concheiro, A.; Madry, H.; Alvarez-Lorenzo, C.; Cucchiari, M. rAAV-mediated overexpression of TGF- $\beta$  via vector delivery in polymeric micelles stimulates the biological and reparative activities of human articular chondrocytes in vitro and in a human osteochondral defect model. *Int. J. Nanomed.* **2017**, *12*, 6985–6996. [[CrossRef](#)]
58. López Arbeloa, F.; López Arbeloa, T.; Tapia Estévez, M.; López Arbeloa, I. Photophysics of rhodamines: Molecular structure and solvent effects. *J. Phys. Chem.* **1991**, *95*, 2203–2208. [[CrossRef](#)]
59. Beija, M.; Afonso, C.A.M.; Martinho, J.M.G. Synthesis and applications of Rhodamine derivatives as fluorescent probes. *Chem. Soc. Rev.* **2009**, *38*, 2410–2433. [[CrossRef](#)]
60. Renny, J.S.; Tomasevich, L.L.; Tallmadge, E.H.; Collum, D.B. Method of continuous variations: Applications of job plots to the study of molecular associations in organometallic chemistry. *Angew. Chem. Int. Ed. Engl.* **2013**, *52*, 11998–12013. [[CrossRef](#)]
61. Benesi, H.A.; Hildebrand, J. A spectrophotometric investigation of the interaction of iodine with aromatic hydrocarbons. *J. Am. Chem. Soc.* **1949**, *71*, 2703–2707. [[CrossRef](#)]
62. Sauer, M.; Han, K.T.; Müller, R.; Nord, S.; Schulz, A.; Seeger, S.; Wolfrum, J.; Arden-Jacob, J.; Deltau, G.; Marx, N.J.; et al. New fluorescent dyes in the red region for biodiagnostics. *J. Fluoresc.* **1995**, *5*, 247–261. [[CrossRef](#)]
63. Savarese, M.; Aliberti, A.; De Santo, I.; Battista, E.; Causa, F.; Netti, P.A.; Rega, N. Fluorescence Lifetimes and Quantum Yields of Rhodamine Derivatives: New Insights from Theory and Experiment. *J. Phys. Chem. A* **2012**, *116*, 7491–7497. [[CrossRef](#)]
64. Zhang, X.-F.; Su, N.; Lu, X.; Jia, W. Benzoate-modified rhodamine dyes: Large change in fluorescence properties due to photoinduced electron transfer. *J. Lumin.* **2016**, *179*, 511–517. [[CrossRef](#)]
65. Mercadé-Prieto, R.; Rodríguez-Rivera, L.; Chen, X.D. Fluorescence lifetime of Rhodamine B in aqueous solutions of polysaccharides and proteins as a function of viscosity and temperature. *Photochem. Photobiol. Sci.* **2017**, *16*, 1727–1734. [[CrossRef](#)]
66. Granadero, D.; Bordello, J.; Pérez-Alvite, M.J.; Novo, M.; Al-Soufi, W. Host-guest complexation studied by fluorescence correlation spectroscopy: Adamantane-cyclodextrin inclusion. *Int. J. Mol. Sci.* **2010**, *11*, 173–188. [[CrossRef](#)]
67. Liénard, R.; Montesi, M.; Panseri, S.; Dozio, S.M.; Vento, F.; Mineo, P.G.; Piperno, A.; De Winter, J.; Coulembier, O.; Scala, A. Design of naturally inspired jellyfish-shaped cyclopolylactides to manage osteosarcoma cancer stem cells fate. *Mater. Sci. Eng. C* **2020**, *117*, 111291. [[CrossRef](#)]
68. Radermacher, J.; Jentsch, D.; Scholl, M.A.; Lustinetz, T.; Frolich, J.C. Diclofenac concentrations in synovial fluid and plasma after cutaneous application in inflammatory and degenerative joint disease. *Br. J. Clin. Pharm.* **1991**, *31*, 537–541. [[CrossRef](#)]
69. Benson, M.D.; Aldo-Benson, M.; Brandt, K.D. Synovial fluid concentrations of diclofenac in patients with rheumatoid arthritis or osteoarthritis. *Semin. Arthritis Rheum.* **1985**, *15*, 65–67. [[CrossRef](#)]
70. McCrea, J.D.; Telford, A.M.; Kaye, C.M.; Boyd, M.W.J. A comparison of plasma and synovial fluid profiles of standard and controlled-release formulations of ketoprofen in patients with rheumatoid arthritis. *Curr. Med. Res. Opin.* **1986**, *10*, 73–81. [[CrossRef](#)]
71. Costa, P.; Sousa Lobo, J.M. Evaluation of Mathematical Models Describing Drug Release from Estradiol Transdermal Systems. *Drug Dev. Ind. Pharm.* **2003**, *29*, 89–97. [[CrossRef](#)]

72. Zambito, Y.; Pedreschi, E.; Di Colo, G. Is dialysis a reliable method for studying drug release from nanoparticulate systems?—A case study. *Int. J. Pharm.* **2012**, *434*, 28–34. [[CrossRef](#)]
73. Bottari, F.; Colo, G.D.; Nannipieri, E.; Saettone, M.F.; Serafini, M.F. Evaluation of a dynamic permeation technique for studying drug-macromolecule interactions. *J. Pharm. Sci.* **1975**, *64*, 946–949. [[CrossRef](#)] [[PubMed](#)]



© 2020 by the authors. Licensee MDPI, Basel, Switzerland. This article is an open access article distributed under the terms and conditions of the Creative Commons Attribution (CC BY) license (<http://creativecommons.org/licenses/by/4.0/>).